Electronic States of *o*-Nitrobenzaldehyde: A Combined Experimental and Theoretical Study

Verónica Leyva,[†,‡] Inés Corral,*[,‡] Thomas Schmierer,[§] Björn Heinz,[§] Ferran Feixas,[||] Annapaola Migani,[||] Lluís Blancafort,[||] Peter Gilch,[§] and Leticia González*[,†,‡]

Institut für Chemie und Biochemie, Freie Universität Berlin, Takustr. 3, 14195 Berlin, Germany, Institut für Physikalische Chemie, Friedrich-Schiller-Universität Jena, Helmholtzweg 4, 07743 Jena, Germany, Fakultät für Physik, Ludwig-Maximilians-Universität München, Oettingenstr. 67, 80538 Munich, Germany, and Institut de Química Computacional, Universitat de Girona, Campus de Montilivi, 17071 Girona, Spain

Received: December 20, 2007; Revised Manuscript Received: February 21, 2008

The experimental UV/vis absorption spectrum of *ortho*-nitrobenzaldehyde (*o*-NBA) has been assigned by means of MS-CASPT2/CASSCF, TD-DFT, and RI-CC2 theoretical computations. Additional information on the nature of the absorbing bands was obtained by comparing the *o*-NBA spectrum with that of related compounds, as, e.g., nitrobenzene and benzaldehyde. For wavelengths larger than ~280 nm, the absorption spectrum of *o*-NBA is dominated by a series of weak nπ^* absorptions from the NO_2 and CHO groups. These weak transitions are followed in energy by a more intense band, peaking at 250 nm and arising from charge transfer $\pi\pi^*$ excitations involving mainly benzene and nitro orbitals. Finally, the most intense band centered at 220 nm has its origin in the overlap of two different absorptions: the first one localized in the NO_2 substituent and the second one arising from a charge transfer excitation involving the NO_2 and the CHO fragments, respectively.

1. Introduction

More than 100 years ago, Ciamician and Silber reported the photo-induced transformation of *ortho*-nitrobenzaldehyde (*o*-NBA) into *ortho*-nitrosobenzoic acid.[1] Their report is regarded as the advent of modern organic photochemistry.[2] However, the elucidation of the mechanism of the "oldest" organic photoreaction had to await the emergence of (highly) time-resolved spectroscopy. In 1980, George and Scaiano[3] observed solvent-dependent transients on the nanosecond time scale and below. Later experiments with higher time resolution led Yip and Sharma[4] to the conclusion that the species with the solvent-dependent lifetime is a ketene. This ketene intermediate would result from a photo-induced hydrogen transfer from the aldehyde substituent to the nitro group. It was then postulated to constitute the first ground-state intermediate in a cascade of reactions yielding the nitroso product. Recently, by means of femtosecond IR spectroscopy some of us have proven the existence of the ketene as an intermediate.[5] This experiment has also revealed that the ketene is formed on an ultrashort time scale of ~400 fs and it is formed in the electronic ground state. This short formation time scale points to an excited singlet state as the precursor of the ketene and strong non-adiabatic effects mediating the decay of the excited state.

From the theoretical point of view, nothing is known about either the assignment of the excited states of *o*-NBA or the mechanism of its photoreaction. Simpler systems, like nitrobenzene and benzaldehyde, have been investigated with multiconfigurational methods in refs 6 and 7, respectively. These calculations are a useful reference point for this work, since they have been carried out at a level of theory comparable to the one used here.

In a joint experimental and theoretical effort, we aim at unravelling the dynamics of the hydrogen transfer reaction in *o*-NBA by means of steady-state as well as time-resolved spectroscopy and quantum mechanical methods. Since hydrogen transfer is assumed to initiate the transformation of most photoreactive nitroarenes[8] our investigation strives for understanding the mechanistic patterns of a very general reaction. As a starting point, we characterize here the adiabatic excited singlet states of *o*-NBA. A tentative assignment based on the experimental absorption spectrum of *o*-NBA and related compounds is first given. The assignment is then supported by computing *o*-NBA with different state of the art quantum chemical methods. Specifically, we have performed multistate second-order perturbation theory on complete active space self-consistent field wavefunctions (MS-CASPT2/CASSCF), time-dependent density functional theory (TD-DFT), and second-order approximate coupled cluster (CC2) calculations.

2. Experimental Methods

UV/vis absorption spectra were recorded using a Lambda 19 spectrometer from Perkin-Elmer. The cyclohexane solvent was of spectroscopic grade (Sigma-Aldrich, Chromasolv). The aromatic compounds (*o*-NBA (Merck, for synthesis), *o*-nitrotoluene (Aldrich, 99+%), *o*-ethylnitrobenzene (Aldrich, 96%), toluene (Merck, Uvasol), and benzaldehyde (Merck, for synthesis)) were used as received. Sample solutions had concentrations of approximately 1 mM. Fused silica cells with a path length of 1–10 mm depending on the sample absorbance were used to record the spectra. The solvent contribution was corrected for by recording solvent blanks. To obtain the gas-phase spectrum of *o*-ethylnitrobenzene, a small drop of the substance was placed in a 50 mm fused silica sample cell. After equilibration between liquid and gas phase, the spectrum was recorded using the empty cell as a blank.

[†] Freie Universität Berlin.
[‡] Friedrich-Schiller-Universität Jena.
[§] Ludwig-Maximilians-Universität München.
[||] Universitat de Girona.

10.1021/jp711949j CCC: $40.75
Published on Web 05/21/2008

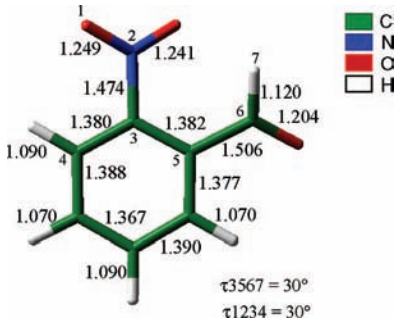

Figure 1. Most relevant geometrical parameters of the experimental structure of *o*-nitrobenzaldehyde.[9] The distances are in angstroms and the angles in degrees.

3. Computational Methods

The electronic calculations for *o*-NBA were performed on the X-ray experimental structure reported by Coppens et al.[9] The relevant geometrical parameters are summarized in Figure 1. In this structure of C_1 symmetry, the NO_2 and CHO substituents are non-coplanar with the aromatic skeleton, lying in planes forming a 30° dihedral angle with respect to the benzene ring.

The theoretical absorption spectrum was calculated at MS-CASPT2/CASSCF[10] level of theory and compared with those obtained using TD-DFT[11] and CC2[12] methods. The TD-DFT calculations were performed using the B3LYP functional combined with the triple zeta quality basis set 6-311G(d,p). Other functionals, namely, PBE and BLYP, were also tested and showed negligible differences in their vertical excited spectra; therefore, results are only reported for the B3LYP functional. The CC2 Franck-Condon excitation energies were calculated using the TZVP basis set and the resolution of the identity (RI) approximation.[13]

The MS-CASPT2/CASSCF calculations have been performed with the atomic natural orbital large basis set, ANO-L,[14] designed for the accurate description of the ionization potentials, electron affinities, and polarizabilities. The following contraction schemes were used: a set of (14s9p4d3f) was contracted to [4s3p2d] for C, O, and N and (8s4p3d)/[3s2p] for H. The initial wavefunctions of the MS-CASPT2/CASSCF protocol were obtained through state average SA-CASSCF calculations performed on six roots with equal weights of A_1 symmetry and were subsequently used as reference in the MS-CASPT2 calculation,[15] which accounts for dynamical correlation effects. In cases where the active space is not complete, intruder states usually arise. To remove intruder states, the level-shift technique[16] with a parameter of 0.3 a.u. was considered. This parameter was chosen after a careful examination of the stability of the excitation energies and the comparison of the excited states reference weight with that of the ground state. Moreover, the reliability of the MS-CASPT2 calculations has been assessed on the basis of the off-diagonal elements of the asymmetric, effective multistate Hamiltonian. These elements should be small, and complementary H_{ij} and H_{ji} elements should have similar values. In the MS-CASPT2/CASSCF(16,12) calculations of Table 2, the off-diagonal elements are smaller than 5 mHartree, and the largest difference between off-diagonal element pairs is 2.5 mHartree. In turn, the multistate correction on the CASPT2 energies is small, less than 1.5 mHartrees for the six states. Thus, the MS-CASPT2 procedure can be safely used here.

In the CASSCF method, the selection of the active orbitals and electrons is the key step to obtain reliable eigenfunctions and eigenenergies. Despite the medium size of *o*-NBA, the choice of the relevant orbitals/electrons is nontrivial and deserves some comment. The complete active space in *o*-NBA should include 24 electrons in 17 orbitals, which comprises the 3 π,π^* orbital pairs of the benzene ring, 1 π,π^* pair of the CO group, 2 π,π^* pairs in the NO_2 group plus a nonbonding P_{NO2} orbital, and the 6 lone pairs (n) on the oxygen atoms of the nitro and carbonyl groups. Such an active space (24,17) is beyond the current computer capabilities, and therefore, several restricted active spaces have been investigated. The tested reduced active spaces include (12,11), (16,12), (16,13), and (18,14). The smallest active space (12,11) excludes all lone pairs, while the biggest active space employed (18,14) includes only one lone pair per oxygen atom. The intermediate active spaces include several lone pairs at the expense of some π,π^* pairs. A detailed composition of the active spaces can be found in Table 1. As will be shown in the next section, TD-DFT and CC2 calculations predict $n\pi^*$ transitions in the low-lying spectral energy region, confirming the key role of the n orbitals. Obviously, the active space (12,11), excluding lone pairs, cannot describe adequately the low-energy part of the *o*-NBA spectrum. On the contrary, the (18,14) active space should be the best affordable choice to describe both $\pi\pi^*$ and $n\pi^*$ transitions simultaneously. Because of the enormous computational effort involved in the calculation of electronic excited states with this active space, the more practicable (16,12) active space was chosen to describe the markedly multiconfigurational character of *o*-NBA (see also next section). This active space is shown in Figure 2a and comprises 16 electrons distributed into 2 pairs of π_{CC} and π^*_{CC} orbitals localized on the benzene moiety, the π_{CO}, π^*_{CO} orbitals, the lone pair n_{CO} from the aldehyde group, 2 nitro lone pair orbitals n_{NO2}, and the bonding, antibonding, and nonbonding π_{NO2}, π^*_{NO2}, and P_{NO2} orbitals from the nitro group. It should be noted, however, that this active space with a small number of roots (vide infra) fails to describe one of the low-lying $\pi\pi^*$ excitations, and thus, this missing state has been calculated with the (12,11) active space that in turn excludes lone pairs (see Figure 2b).

All the MS-CASPT2/CASSCF calculations were performed using the *MOLCAS 6.0* quantum chemistry software,[17] while TD-DFT and RI-CC2 calculations were carried out with the *Gaussian03*[18] and *TURBOMOLE* (v 5.7)[19] suite of programs, respectively.

4. Results and Discussion

4.1. Active Space Dependence. Before assigning the experimental absorption spectrum of *o*-NBA with the help of the theoretical results, we shall shortly comment on the dependence of the vertical excitation energies and order of the states when using different active spaces in the MS-CASPT2 methodology. Also, we will justify the use of different active spaces when rationalizing the complete low-energy part of the absorption spectrum. Figure 3 is a summary of the results obtained with the different active spaces embodied in Table 1. As anticipated, the vertical spectrum calculated with the (12,11) active space is exclusively dominated by $\pi\pi^*$ excitations localized in the aromatic ring, CT excitations, or a mixture of both. The inclusion of two (i.e., (16,13) active space) or more (i.e., (16,12) active space) lone pairs from the NO_2 or the carbonyl group orbitals introduces $n\pi^*$ excitations in the low-energy region of the spectrum. Note that the active space (16,12) includes three lone pairs at the expense of removing a $\pi\pi^*$ pair, with respect to the (12,11) and (16,13) active spaces; see Table 1. As can be seen from Figure 3, the excitation energies for the $n\pi^*$ tran-

TABLE 1: Composition of the CASSCF Active Spaces Employed in This Work

	π_{CC}	π_{CC}	π_{CC}	π_{CO}	π_{NO2}	P_{NO2}	n_{NO2}	n_{NO2}	n_{NO2}	n_{NO2}	n_{CO}	n_{CO}	π^*_{NO2}	π^*_{CO}	π^*_{CC}	π^*_{CC}	π^*_{CC}
(12,11)	X	X	X	X	X	X							X	X	X	X	X
(16,12)		X	X	X	X	X	X	X			X		X	X	X	X	
(16,13)	X	X	X	X	X	X	X	X					X	X	X	X	X
(18,14)	X	X	X	X	X	X	X	X			X		X	X	X	X	X

TABLE 2: CASSCF and MS-CASPT2 Vertical Excited Spectra and Single Components of the Gaussian Decomposition of the Experimental Spectrum of *o*-Nitrobenzaldehyde in Cyclohexane[a]

	CASSCF/ANO-L					MS-CASPT2/ANO-L					exp. abs. spectrum		
state	configuration	CI coeff	ΔE (eV)	ΔE (nm)	f	configuration	CI coeff	ΔE (eV)	ΔE (nm)	f	abs.band (nm)	Gauss. center (nm)	Gauss.f
S_1	$n_{NO2} \rightarrow \pi^*_{NO2}$	−0.43	3.77	329	0.0027	$\pi_{CC1} \rightarrow \pi^*_{NO2}$	−0.41	3.33	372	0.0026	300	337	0.008
	$\pi_{CC1} \rightarrow \pi^*_{NO2}$	−0.40				$n_{NO2} \rightarrow \pi^*_{NO2}$	−0.40						
S_2	$n_{CO} + n_{NO2} \rightarrow \pi^*_{NO2}$	−0.61	4.65	267	0.0005	$n_{CO} + n_{NO2} \rightarrow \pi^*_{CC} + \pi^*_{CO}$	−0.43	3.82	324	0.0000		292	0.030
	$n_{CO} - n_{NO2} \rightarrow \pi^*_{NO2}$	−0.37				$n_{CO} + n_{NO2} \rightarrow \pi^*_{NO2}$	−0.42						
S_3	$n_{NO2} \rightarrow \pi^*_{NO2}$	0.61	4.29	289	0.0001	$n_{NO2} \rightarrow \pi^*_{NO2}$	0.52	3.88	319	0.0006			
	$n_{CO} + n_{NO2} \rightarrow \pi^*_{NO2}$	−0.45				$n_{CO} + n_{NO2} \rightarrow \pi^*_{CC} + \pi^*_{CO}$	0.42						
S_4	$\pi_{CC2} \rightarrow \pi^*_{NO2}$	−0.37	6.01			$\pi_{CC2} \rightarrow \pi^*_{NO2}$	−0.36				250	261	0.078
	$\pi_{CC2} \rightarrow \pi^*_{CC} - \pi^*_{NO2}$	0.36				$\pi_{CC2} \rightarrow \pi^*_{CC} - \pi^*_{NO2}$	0.36	4.45	278	0.0147			
	$\pi_{CC1} \rightarrow \pi^*_{CC} + \pi^*_{CO}$	−0.35				$\pi_{CC1} \rightarrow \pi^*_{CC} + \pi^*_{CO}$	−0.34						
S_5	$P_{NO2} \rightarrow \pi^*_{CC} + \pi^*_{NO2}$	−0.58	7.07	175	0.2447	$P_{NO2} \rightarrow \pi^*_{CC} + \pi^*_{NO2}$	−0.52	4.94	251	0.2269		248	0.047
	$\pi_{CC1} \rightarrow \pi^*_{CC} + \pi^*_{NO2}$	0.45				$\pi_{CC1} \rightarrow \pi^*_{CC} + \pi^*_{NO2}$	0.54						
S_6	$P_{NO2} \rightarrow \pi^*_{NO2}$	0.54	6.59	188	0.0550	$P_{NO2} \rightarrow \pi^*_{NO2}$	0.53	5.55	223	0.0469	220	225	0.250
S_7												204	0.420

[a] All bands are obtained with a (16,12) reference active space, except S_5, which is obtained with a (12,11) active space (see Table 1 for details). Corresponding orbitals in Figure 2.

sitions provided by the (16,12) and (16,13) active spaces agree with each other satisfactorily. Because of the prohibitive cost of the (18,14) active space, our calculation is restricted to the estimation of the CASSCF transition energy for the first singlet excited state (not included in Figure 3). It is worth mentioning that this energy compares reasonably well with that obtained with CAS (16,12) and CAS (16,13), which are underestimated by 0.3 and 0.2 eV, respectively. The lack of n_{CO} lone pairs of the (16,13) active space, however, prevents it from predicting the existence of a third $n\pi^*$ excited state calculated at 3.82 eV by the (16,12) active space. This state consists of the following one electron excitations: $n_{CO} + n_{NO2} \rightarrow \pi^*_{CC} + \pi^*_{CO}$ and $n_{CO} + n_{NO2} \rightarrow \pi^*_{NO2}$. In the region from 4 to 6 eV, the smaller active space, namely, (12,11), predicts the existence of three $\pi\pi^*$ states at 4.48, 4.94, and 5.73 eV. Only the first and third of them are described in this region with the SA calculations over 6 and 5 roots performed with the active spaces (16,12) and (16,13), respectively. The second low-lying $\pi\pi^*$ state does not appear with these active spaces and the chosen number of roots. This state can only be described when using 10 roots; however, the inclusion of such a high number of states introduces several double excitations that lead to a worsening of the SA orbitals and remaining excitation energies. Therefore, henceforth we restrict ourselves to the results obtained with the (16,12) active space and 6 roots.

4.2. Absorption Spectrum of *o*-NBA. Experimental spectra were recorded in a nonpolar aprotic solvent (cyclohexane) to minimize solute−solvent interactions and allow for a better comparison with the gas-phase calculations discussed below. To roughly quantify the residual solvent effect, the gas-phase spectrum of *o*-Ethylnitrobenzene (*o*-ENB) was compared to the one in solution (Figure 4). *o*-ENB was chosen since its vapor pressure is appreciable at room temperature. Gas- and solution-phase spectra resemble each other in shape. Weak absorption bands at longer wavelengths are followed by stronger ones in the deeper UV region. In general, the solution-phase spectrum is shifted towards longer wavelengths. The magnitude of this shift depends on the nature of the considered band. In the case of *o*-ENB, the maximal shift observed is around 15 nm (∼0.3 eV) for the band at ∼250 nm. Solvent-induced shifts of this magnitude must be allowed for when comparing condensed-phase experimental and gas-phase computed spectra.

The experimental absorption spectrum of *o*-NBA recorded in cyclohexane (see Figure 5a) shows several overlapping bands. Maxima of three distinct bands centered at 220, 250, and 300 nm can be directly discerned. Further bands and exact band positions were extracted by a Gaussian decomposition. A Gaussian decomposition is justified as follows: For a *single* vibronic transition, one expects a Lorentzian line shape for purely homogeneous broadening, a Gaussian one for purely inhomogeneous, and a Voigt profile for an intermediate case.[20] In the present case, broadenings—either homogeneous or inhomogeneous—completely smear out the vibrational progression, i.e., single vibronic transitions are not resolved. Under these circumstances, the line shape function has to represent a vibrational envelope. As an approximation for this (complex) envelope, Gaussian and Lorentzian trial functions have been suggested (for a recent review, see ref 21). Here, in line with ref 21, Gaussian functions are better suited than Lorentzian ones. Such a procedure requires at least five Gaussian components. A very good agreement is obtained when using six components (Figure 6). For each Gaussian component i, the oscillator strength f_i was calculated according to[22]

$$f_i = 4.32 \cdot 10^{-9} \int \varepsilon_i(\tilde{\nu})\, \mathrm{d}\tilde{\nu}$$

Hereby, ϵ_i is the extinction coefficient measured in units M^{-1} cm^{-1} as a function of wavenumber $\tilde{\nu}$. The center frequencies and the oscillator strengths are compiled in Figure 6 and Table 2. Information about the origin of these bands can be obtained from the comparison of the absorption spectrum of *o*-NBA with that of related compounds, namely, *o*-nitrotoluene (*o*-NT), *o*-ethylnitrobenzene (*o*-ENB), benzaldehyde, and toluene (Figure 5). For wavelengths larger than ∼230 nm, the spectrum of *o*-NBA bears strong similarities to those of *o*-NT and *o*-ENB. Considerable differences are observed when comparing the

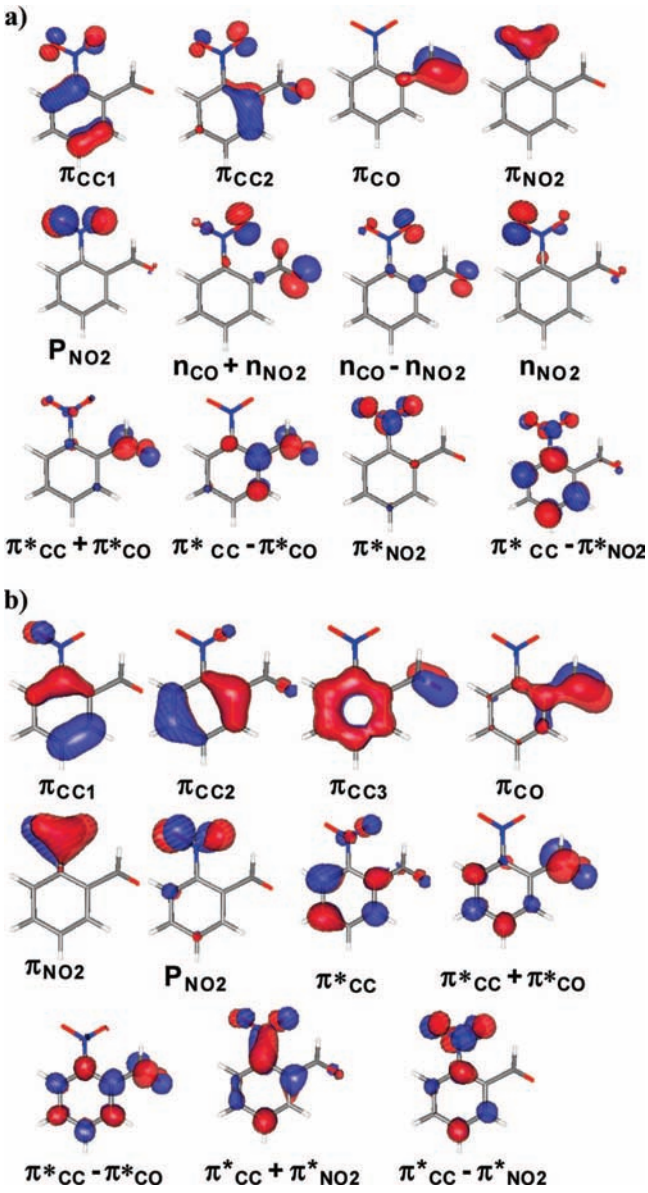

Figure 2. Molecular orbitals included in the (16,12) (a) and the (12,11) (b) active spaces of the SA-CASSCF/ANO-L calculations over six (a) and five (b) roots, respectively.

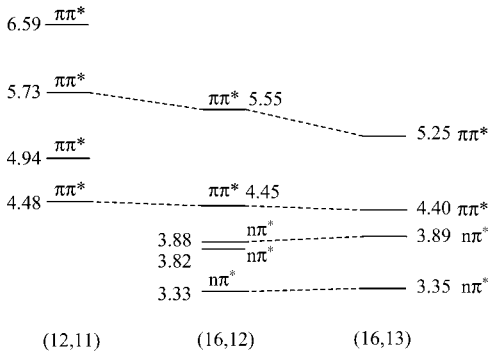

Figure 3. Relative MS-CASPT2 excitation energies (in eV) and state ordering employing different active spaces.

spectrum of *o*-NBA with that of toluene. Generally, the extinction coefficients of toluene are much smaller than those of all other compounds throughout the spectral range covered. Furthermore, vibrational progressions in toluene are recorded, whereas they are not resolved in the nitroarenes. From that, one

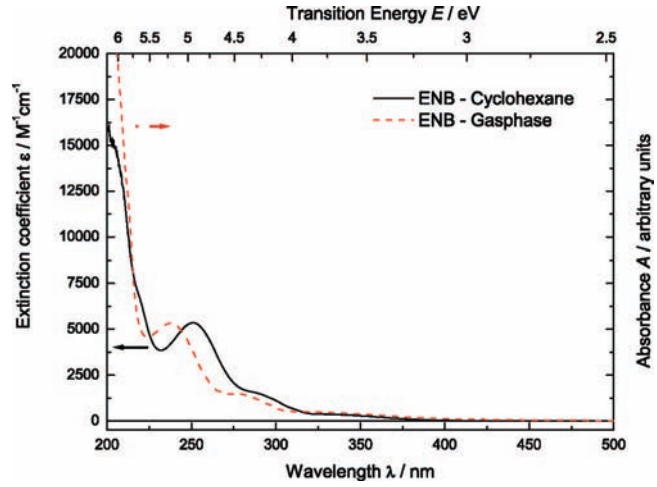

Figure 4. Experimental absorption spectrum of *o*-Ethylnitrobenzene (ENB) in the gas phase and in cyclohexane solution. For ENB in solution, the ordinate gives the extinction coefficient ϵ as a function of the wavelength λ. The gas-phase spectrum has been arbitrarily scaled for an easy comparison.

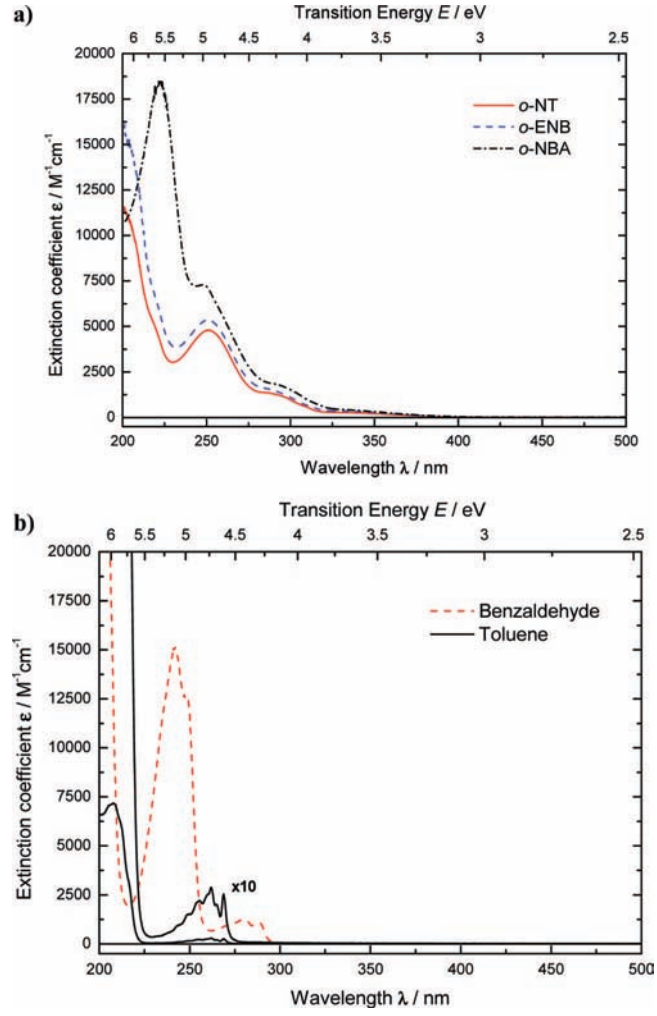

Figure 5. Absorption spectra of some nitroarenes (*o*-NBA, *o*-NT, *o*-ENB, part a) and toluene and benzaldehyde (part b) all dissolved in cyclohexane. In all spectra, the extinction coefficient ϵ is plotted as a function of the wavelength λ.

can deduce that the benzene ring alone is not responsible for the absorption properties of *o*-NBA. Benzaldehyde features an intense absorption band around 230 nm and a weak absorption

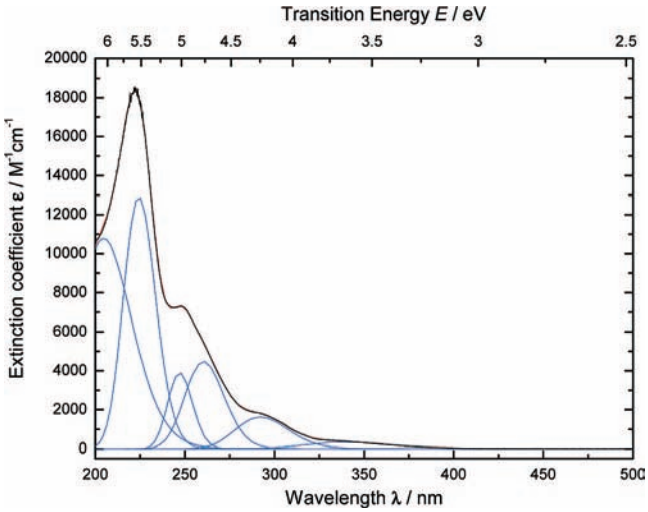

Figure 6. Experimental absorption spectrum (in black) and its Gaussian decomposition (single components in blue and their sum in red) of *o*-NBA in cyclohexane. The spectrum is represented with a linear wavelength scale. Gaussian fitting was done employing a linear frequency (or energy) scale.

that spreads from 275 to 300 nm; see Figure 5b. By allowing for small shifts, these bands might be related—at least partially—to the intense band at 220 nm and to the broad band peaking at 300 nm of *o*-NBA, respectively.

Hence, the low-energy part of the *o*-NBA spectrum (250–350 nm) could in principle be related to the excited states of benzaldehyde and nitrobenzene or to excitations that involve the nitro and carbonyl group chromophores simultaneously. Other spectral properties of *o*-NBA should be attributable to the nitrobenzene moiety. Indeed, the gas-phase spectrum of nitrobenzene[23] strongly resembles those of the nitroarenes investigated here. It shows a couple of weak transitions at long wavelengths above 270 nm and a rather strong ($\epsilon = 8500$ M^{-1} cm^{-1}) one at 240 nm.[23]

To further assign the experimental bands of *o*-NBA, theoretical calculations in the gas phase have been performed. The Frank-Condon excitation energies and their associated oscillator strengths calculated at MS-CASPT2/CASSCF(16,12), TD-DFT, and CC2 levels of theory are reported in Tables 2, 3, and 4, respectively. In Table 2, the experimental Gaussian centered at 248 nm is assigned on the basis of a MS-CASPT2/CAS SCF(12,11) calculation (see section 4.1).

For an easier comparison among the different methods, the computed spectral data are summarized as stick spectra in Figure 7. The results of the Gaussian decomposition (cf. Figure 6) of the experimental spectrum of *o*-NBA are also included. When comparing the experimental and computed spectra, two facts should be kept in mind. First, the Gaussian decomposition relies on the fact that every absorbing transition leads to a band that can be approximated by a Gaussian-shaped function. The overlap of these Gaussians results in the experimental absorption bands. Deviation of the real band shape from the Gaussian one can result in systematic errors. Secondly, the experimental spectrum was obtained in solution, and thus, spectral shifts of up to 0.3 eV are possible. With these facts in mind, we now proceed to assign the experimental Gaussian decomposition to the excited states of *o*-NBA theoretically calculated.

Comparing the position and oscillator strengths of the six fitted Gaussians with our more reliable MS-CASPT2/CASSCF vertical excitation energies and oscillator strengths, we can relate the Gaussians peaking at 261, 248, and 225 nm to the theoretical

TABLE 3: TD-B3LYP/6-311G(d,p) Transition Energies ΔE (eV, nm), Main One Electron Excitations, Weights, and Oscillator Strengths *f* of the Lower-Lying Electronic States of *o*-Nitrobenzaldehyde[a]

	TD-B3LYP/6-311G(d,p)				
state	weight	configuration	ΔE (eV)	E (nm)	f
S_1	0.635	$n_{CO} \rightarrow \pi^*_{CC} + \pi^*_{NO2}$	3.31	374	0.0006
S_2	−0.397	$n_{NO2}2 \rightarrow \pi^*_{CC} + \pi^*_{NO2}$	3.77	329	0.0124
	0.465	$\pi_{CC1} \rightarrow \pi^*_{CC} + \pi^*_{NO2}$			
S_3	0.346	$n_{NO2}1 \rightarrow \pi^*_{CC} + \pi^*_{NO2}$	4.15	299	0.0044
	0.449	$n_{CO} \rightarrow \pi^*_{CC} + \pi^*_{CO}$			
S_4	0.494	$\pi_{CC2} \rightarrow \pi^*_{CC} + \pi^*_{NO2}$	4.28	289	0.0149
	0.331	$n_{CO} \rightarrow \pi^*_{CC} + \pi^*_{CO}$			
S_5	0.491	$n_{NO2}1 \rightarrow \pi^*_{CC} + \pi^*_{NO2}$	4.46	278	0.0126
	0.307	$\pi_{CC2} \rightarrow \pi^*_{CC} + \pi^*_{NO2}$			
S_6	0.451	$n_{NO2}2 \rightarrow \pi^*_{CC} + \pi^*_{NO2}$	4.82	257	0.1021
	0.400	$\pi_{CC1} \rightarrow \pi^*_{CC} + \pi^*_{NO2}$			
S_7	0.531	$\pi_{CC1} \rightarrow \pi^*_{CC} + \pi^*_{CO}$	5.15	241	0.0267
S_8	0.512	$\pi_{CC2} \rightarrow \pi^*_{CC} + \pi^*_{CO}$	5.43	229	0.1106
S_9	0.512	$P_{NO2} \rightarrow \pi^*_{CC} + \pi^*_{NO2}$	5.65	219	0.0143
	0.348	$P_{NO2} \rightarrow \pi^*_{CC} + \pi^*_{CO}$			
S_{10}	0.589	$n_{CO} \rightarrow \pi^*_{CC} - \pi^*_{NO2}$	5.75	216	0.0066
S_{11}	0.446	$n_{NO2}1 \rightarrow \pi^*_{CC} + \pi^*_{CO}$	5.78	215	0.0409
	0.429	$n_{NO2}2 \rightarrow \pi^*_{CC} + \pi^*_{CO}$			
S_{12}	0.438	$n_{NO2}1 \rightarrow \pi^*_{CC} + \pi^*_{CO}$	5.80	214	0.1110

[a] Corresponding orbitals in Figure 8a.

TABLE 4: RI-CC2/TZV(P) Transition Energies ΔE(eV, nm), Main One-Electron Excitations, CI Coefficients, And Oscillator Strengths, *f*, of the Low-Lying Electronic States of *o*-Nitrobenzaldehyde[a]

	RI-CC2/TZV(P)				
state	configuration	coeff	ΔE (eV)	ΔE (nm)	f
S_1	$n_{NO2}2 \rightarrow \pi^*_{CC} + \pi^*_{NO2}$	0.5870	3.62	343	0.0117
	$n_{NO2}1 \rightarrow \pi^*_{CC} + \pi^*_{NO2}$	−0.5151			
S_2	$n_{NO2}1 \rightarrow \pi^*_{CC} + \pi^*_{NO2}$	0.5734	4.09	303	0.0014
	$n_{NO2}2 \rightarrow \pi^*_{CC} + \pi^*_{NO2}$	0.5182			
S_3	$n_{CO} \rightarrow \pi^*_{CC} + \pi^*_{NO2}$	0.5545	4.11	301	0.0038
	$n_{CO} \rightarrow \pi^*_{CC} + \pi^*_{CO}$	0.5379			
S_4	$\pi_{CC2} \rightarrow \pi^*_{CC} + \pi^*_{NO2}$	0.7093	4.57	271	0.0072
	$\pi_{CC1} \rightarrow \pi^*_{CC} + \pi^*_{CO}$	0.4634			
S_5	$n_{CO} \rightarrow \pi^*_{CC} + \pi^*_{NO2}$	−0.6777	4.95	250	0.0145
	$n_{CO} \rightarrow \pi^*_{CC} + \pi^*_{CO}$	0.4940			
S_6	$\pi_{CC1} \rightarrow \pi^*_{CC} + \pi^*_{NO2}$	0.8428	5.30	234	0.1335
S_7	$\pi_{CC1} \rightarrow \pi^*_{CC} + \pi^*_{CO}$	0.6331	5.82	213	0.0872
	$\pi_{CC2} \rightarrow \pi^*_{CC} + \pi^*_{CO}$	−0.4863			
S_8	$P_{NO2} \rightarrow \pi^*_{CC} + \pi^*_{NO2}$	0.6157	6.20	200	0.1421
	$\pi_{CC2} \rightarrow \pi^*_{CC} + \pi^*_{CO}$	−0.5575			
S_9	$\pi_{CC2} \rightarrow \pi^*_{CC} + \pi^*_{CO}$	−0.5810	6.21	200	0.2038
	$P_{NO2} \rightarrow \pi^*_{CC} + \pi^*_{NO2}$	−0.5585			
S_{10}	$n_{CO} \rightarrow \pi^*_{CC} - \pi^*_{NO2}$	0.5835	6.31	197	0.0050
S_{11}	$\pi_{CC2} \rightarrow \pi^*_{CC} + \pi^*_{CO}$	0.3996	6.55	189	0.1556
	$n_{NO2}1 \rightarrow \pi^*_{CC} + \pi^*_{CO}$	−0.3719			
S_{12}	$n_{NO2}2 \rightarrow \pi^*_{CC} + \pi^*_{CO}$	0.6714	6.73	184	0.0233
S_{13}	$n_{NO2}1 \rightarrow \pi^*_{CC} + \pi^*_{CO}$	0.5237	6.88	180	0.0781

[a] Corresponding orbitals in Figure 8b.

absorptions at 278, 251, and 223 nm, respectively (see Table 2 and Figure 7). In general, the corresponding states have $\pi\pi^*$ character. The transition calculated at 278 nm, which is the lowest $\pi\pi^*$ state, is a mixture of a $\pi_{CC2} \rightarrow \pi^*_{CC} - \pi^*_{NO2}$ excitation inside the benzene ring and two charge transfer (CT) excited states, namely, $\pi_{CC2} \rightarrow \pi^*_{NO2}$ and $\pi_{CC1} \rightarrow \pi_{CC} + \pi^*_{CO}$ (see Figure 2a). The considerable mixing of the orbitals involved in the excited states and the marked multiconfigurational character of the wavefunctions, previously observed in other

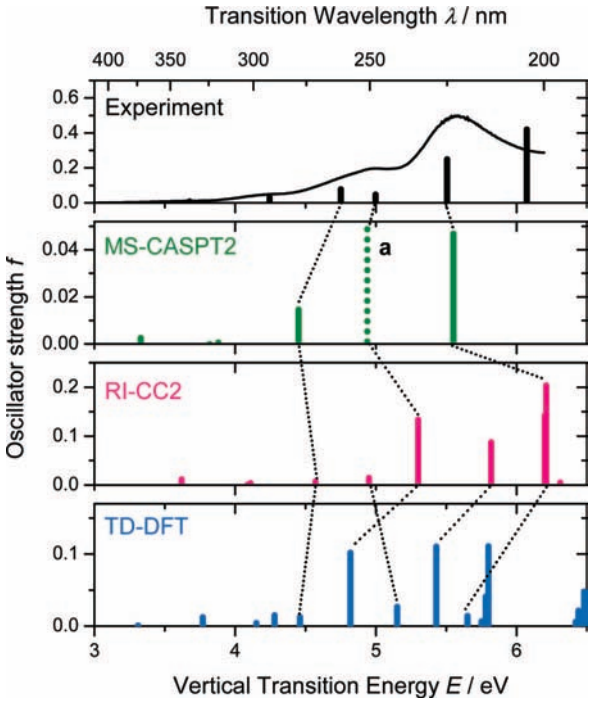

Figure 7. Comparison of the experimental and computed spectra of *o*-NBA. The upper panel shows the experimental spectrum and its Gaussian decomposition in stick representation (the height of a stick represents the oscillator strength *f*). The lower panels show the stick spectra obtained by the computational methods indicated. (a) Indicates band calculated with the (12,11) active space. See text for details.

theoretical nitroarene studies,[6] makes it difficult to assign a predominant one-electron excitation to these transitions. This state calculated at 278 nm can also be interpreted as a combination of the excited states of benzaldehyde and nitrobenzene, which have their lowest calculated $\pi\pi^*$ transitions at 286 and 282 nm, respectively.[6,7] Indeed, the orbitals involved in the $\pi_{CC1} \rightarrow \pi^*_{CC} + \pi^*_{CO}$ configuration of *o*-NBA compare with the ones calculated for the $2^1A'$ state in benzaldehyde.[7]

The experimental Gaussian at 248 nm is not described within the six roots MS-CASPT2/CASSCF(16,12) calculation, but it is present in the vertical excited spectrum calculated with the smaller active space (12,11); recall Figure 3. Our calculations performed with the (12,11) active space predict this state to appear at 251 nm—in good agreement with the experiment. It is a mixture of two main $\pi\pi^*$ transitions, the first localized within the benzene ring and the second of CT involving the nitro group and the antibonding orbitals of benzene. The relevant orbitals for this state are shown in Figure 2b. Accordingly, the difference dipole moment vector with respect to the ground state is parallel to the C_3-N_2 axis and amounts to 3.7 Debye. This transition can be related to the band calculated at 248 nm for nitrobenzene, which shows a similar change in the dipole moment.[6]

Finally, the band calculated at 223 nm involves mainly two orbitals localized in the nitro group. Its counterpart in nitrobenzene should be the 2^1B_2 state,[6] which is calculated at 222 nm; nevertheless, the different shapes of the orbitals in *o*-NBA and nitrobenzene make it difficult to establish a clear-cut correspondence. Note that the highest Gaussian resolved experimentally at 204 nm cannot be predicted by MS-CASPT2 due to the limitations associated with the calculated number of roots and the size of the active spaces employed. This peak will be discussed later with the help of linear response calculations.

According to MS-CASPT2 calculations, the lowest-energy experimental tail with Gaussians resolved at 292 and 337 nm can be interpreted as the overlap of three weakly absorbing transitions of predominant $n\pi^*$ character localized either in the NO_2 or the CHO moiety, that appear at 372, 324, and 319 nm, respectively. Similar to the S_4 state, the three $n\pi^*$ states stem from the combination of transitions occurring in nitrobenzene and benzaldehyde. Specifically, these states are mixtures of the two lowest $n\pi^*$ transitions of nitrobenzene and the 1A″ state of benzaldehyde, which have been calculated between 347 and 299 nm.[6,7] However, the loss of planarity of the substituents in *o*-NBA induces a significant mixing with a $\pi\pi^*$ state, especially in S_1 (see the configurations in Table 2), which results in an increase of the calculated oscillator strength.

TABLE 5: Leading Configurations for the Low-Lying Excited States of NBA at the TD-B3LYP/6-311G(d,p), RI-CC2/TZV(P), and MS-CASPT2/ANO-L Levels of Theory, Respectively

configuration	TD-DFT	RI-CC2	MS-CASPT2
$n_{CO} \rightarrow \pi^*_{CC} + \pi^*_{NO2}$	S_1	S_3, S_5	S_2
$n_{NO2}2 \rightarrow \pi^*_{CC} + \pi^*_{NO2}$	S_2, S_6	S_1, S_2	S_2
$n_{NO2}1 \rightarrow \pi^*_{CC} + \pi^*_{NO2}$	S_3, S_5	S_1, S_2	S_1, S_3
$n_{CO} \rightarrow \pi^*_{CC} + \pi^*_{CO}$	S_4	S_3, S_5	S_2, S_3
$\pi_{CC1} \rightarrow \pi^*_{CC} + \pi^*_{NO2}$	S_2, S_6	S_6	S_1, S_5
$\pi_{CC2} \rightarrow \pi^*_{CC} + \pi^*_{NO2}$	S_4, S_5	S_4	S_4
$\pi_{CC1} \rightarrow \pi^*_{CC} + \pi^*_{CO}$	S_7	S_7	S_4
$\pi_{CC2} \rightarrow \pi^*_{CC} + \pi^*_{CO}$	S_8	S_8, S_9	—
$P_{NO2} \rightarrow \pi^*_{CC} + \pi^*_{NO2}$	S_9	S_8, S_9	S_5

Hereafter, we present the results obtained with the two response methods CC2 and TD-DFT and their comparison with the previous MS-CASPT2 results. To facilitate the interpretation and comparison of CC2 and TD-DFT spectra, the leading configurations of the lowest excited states for the three methods have been summarized in Table 5. It is worth noting that the low-lying states predicted by the three methods involve the same molecular orbitals (compare Figures 2 and 8). From the examination of Tables 3, 4, and 5, we can learn that for wavelengths larger than 200 nm the TD-DFT and RI-CC2 spectra are composed of nine states that in turn appear as linear combinations of nine different configurations: four of $n\pi^*$ type and five showing a $\pi\pi^*$ character (see first column Table 5). The four $n\pi^*$ configurations are responsible for the lowest-absorbing electronic states. Among these configurations, one exhibits a clear CT character between the two substituents ($n_{CO} \rightarrow \pi^*_{CC} + \pi^*_{NO2}$), whereas the other three configurations show a CT character from one of the lone pairs into a π^*_{CC} orbital of the benzene ring. At the RI-CC2 level, these configurations generate four $n\pi^*$ states (S_1-S_3 and S_5), which span from 343 to 250 nm (see Table 4). In the case of TD-DFT, the $n\pi^*$ configurations mix with several $\pi\pi^*$ configurations and therefore are present in six electronic states (see Table 3). As already discussed above, only three low-lying $n\pi^*$ states were found at the MS-CASPT2 level. Inspection of the CASSCF virtual orbitals (recall Figure 2a) shows that the $\pi^*_{CC} + \pi^*_{CO}$ orbital is probably not well-described at this level, due to the absence of one of the π^* orbitals of the benzene ring in the active space (compare the shape of this orbital from the three methods in Figures 2a and 8a,b). This would be the reason why CASSCF and CASPT2 calculations fail to predict the existence of the fourth low-lying $n\pi^*$ state.

The remaining five configurations are of the $\pi\pi^*$ type. Four of them correspond to a partial CT from the benzene ring (π_{CC1} and π_{CC2} orbitals) to the nitro ($\pi^*_{CC} + \pi^*_{NO2}$) and aldehyde ($\pi^*_{CC} + \pi^*_{CO}$) orbitals. The fifth $\pi\pi^*$ configuration corresponds approximately to a local excitation within the nitro group. In all methods employed, the two lowest $\pi\pi^*$ states (S_4 and S_5 in

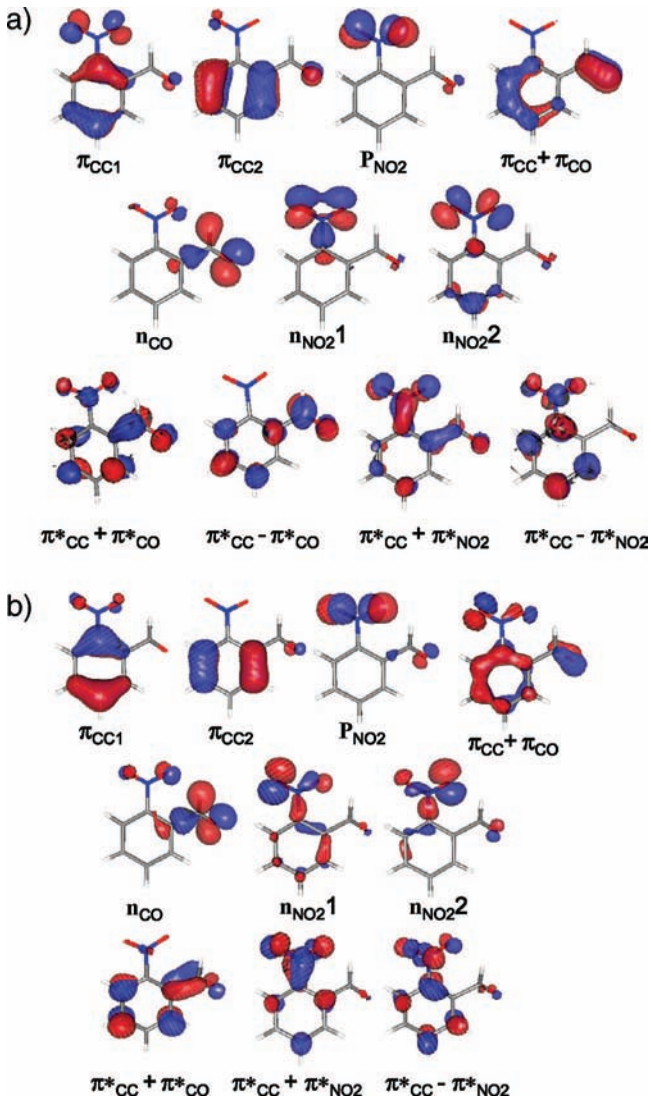

Figure 8. Relevant TD-B3LYP (a) and CC2 (b) molecular orbitals for the interpretation of NBA's vertical excited spectrum.

MS-CASPT2, S_4 and S_6 in CC2, and S_5 and S_6 in TD-DFT) are mainly composed of the two benzene → nitro transitions, although at the TD-DFT and MS-CASPT2 levels, these states are mixed with other configurations. The next $\pi\pi^*$ states are benzene → aldehyde transitions at the RI-CC2 (S_7, S_8, and S_9) and TD-DFT (S_7 and S_8) levels of theory with certain mixings. Specifically, at RI-CC2 the S_8 and S_9 states are mixed with the $P_{NO2} \rightarrow \pi^*_{CC} + \pi^*_{NO2}$ configuration.

These configurations are poorly represented with MS-CASPT2, once more, because of the lack of flexibility of the active space to properly describe the $\pi^*_{CC} + \pi^*_{CO}$ orbital. This is why these two electronic states have no counterpart in MS-CASPT2 theory. The difficulty in describing the benzene → aldehyde transitions may also explain the loss of quality of the wave function when more roots are included. Finally, the local nitro group transition (S_6 at MS-CASPT2, $S_8 + S_9$ CC2, and S_9 TD-DFT) is predicted by the three methods to give rise to states higher in energy than the benzene → nitro and benzene → aldehyde transitions.

Beyond the S_9 excited state, CC2 and TD-DFT methods predict a weakly absorbing CT state involving the aldehyde lone pair and the benzene molecular orbital $\pi^*_{CC} - \pi^*_{NO2}$ at 197 and 216 nm, respectively. More intense is, however, the state that follows in energy, which presents a $n_{NO2} \rightarrow \pi^*_{CC} + \pi^*_{CO}$ character. None of these two states is, however, present in the MS-CASPT2 spectrum due to, on one hand, the limitation of the number of roots calculated and, on the other hand, the poor description of the $\pi^*_{CC} + \pi^*_{CO}$ orbital by this method. In view of the oscillator strength predicted by CC2 theory for this electronic state peaking at 189 nm (CC2), we assign the Gaussian band calculated at 204 nm from the experimental spectrum to a $n_{NO2} \rightarrow \pi^*_{CC} + \pi^*_{CO}$ transition (see Table 4).

From the former analysis, we can conclude that the composition of the low-lying excited states predicted by the three methods employed here is based on the same nine configurations, although important differences are found in the way the different configurations combine to yield the respective electronic states. It is also worth highlighting that the three methods considered report the same state ordering for the calculated electronic states, even if positions and oscillator strengths of the excited states change in some cases from method to method. An interpretation of the experimental spectrum of *o*-NBA has to take these facts into account. In general, the non-negligible multireference character of the ground-state wavefunction imposes the use of CASSCF-based methods, with their inherent limitation on the size and choice of the active space. The response methods can complement the information missed by the MS-CASPT2/CASSCF theory, but caution must be exercised in the interpretation of TD-DFT, which lacks accuracy, especially when treating CT states. Still, on the basis of our complementary findings an assignment seems possible and reads as follows: The weak experimental absorption band ranging from 400 to 280 nm stems from the overlap of four different $n\pi^*$ excitations from the lone pairs of the nitro and aldehyde groups into benzene π^*_{CC}, π^*_{CO}, and π^*_{NO2} orbitals. The experimental absorption band centered at 250 nm arises from the joint absorption of two CT π (benzene) → π^* (nitro) transitions. Finally, the intense experimental band at 220 nm is the result of an overlap of two $\pi\pi^*$ excitations located in the same frequency range, one within the NO_2 moiety and a second one involving a CT $n_{NO2} \rightarrow \pi^*_{CC} + \pi^*_{CO}$ transition. According to our calculations, contributions from π (benzene) → π^* (aldehyde) to the experimental bands at 250 and 220 nm are also expected.

5. Conclusions

This paper reports on the analysis of the electronic absorption spectrum of *o*-NBA, based on highly correlated quantum chemical calculations and the comparison of the experimental *o*-NBA spectrum with those of other nitroarenes, toluene, and benzaldehyde.

In general, the three theoretical methods considered in this work, namely, MS-CASPT2/CASSCF, CC2, and TD-DFT, lead to a consistent assignment of the experimental absorption spectrum of *o*-NBA. They predict the lowest-lying electronic excited states as linear combinations of the same nine electronic configurations. Still, the weight of the configurations inside each electronic state differs in some cases from one method to the other, and some discrepancies are found concerning the positions and oscillator strengths of the absorbing states. Nevertheless, the state ordering provided by the three methods is maintained. Taking into account the markedly multiconfigurational character of the ground-state wavefunction and the importance of the CT transitions in the low-energy region of the *o*-NBA spectrum, we propose the following assignment of the experimental spectrum. The very broad tail in the *o*-NBA spectrum peaking at 300 nm is assigned to the absorption of several $n\pi^*$ excitations involving π^* orbitals localized either in the benzene

ring or in the NO_2 and the CHO moieties. In the range between 270 and 240 nm, two CT π (benzene) $\rightarrow \pi^*$ (nitro) absorptions were calculated. The experimentally observed intense band around 220 nm corresponds to the superposition of two intense states, the first one being a $\pi\pi^*$ state localized within the NO_2 group and the second one being an $n\pi^*$ state involving a CT excitation from the nitro to the aldehyde group. Finally, our calculations predict π (benzene) $\rightarrow \pi^*$ (aldehyde) contributions for the two most intense bands of the spectrum.

In view of the ultrafast hydrogen transfer measured for *o*-NBA after excitation at 260 nm,[5] one might expect a reactive state around this wavelength. Relaxation on such a state would lead to the hydrogen transfer. According to our calculations, such a reactive state could be any of the CT states involving the benzene and the nitro moieties. As a response to neutralize the generated charges induced by the CT state, the hydrogen transfer is the result of a proton which follows the electron. A possible reactive state is the $\pi\pi^*$ state that appears at 251 nm in the MS-CASPT2 calculation, since it has a significant charge transfer to the nitro group. In this state, the virtual orbital that acts as electron "acceptor" has the signature of the bonding pattern of the primary ketene photoproduct (double bond between the nitrogen and the adjacent carbon; see orbital $\pi^*_{CC} + \pi^*_{NO2}$ of Figure 2b). Alternatively, and following Kasha's rule and in accordance with the hints provided by, e.g., ref 3, the reaction could take place after an initial rapid internal conversion relaxation on the lowest excited state surface. This would lead to population of an $n\pi^*$ state located at the nitro group. Such a state features a hole in a lone pair of this group, which might attract the hydrogen located at the aldehyde function of *o*-NBA, triggering the photoreaction. Calculations to obtain minimum-energy paths and relaxation pathways in *o*-NBA are in progress to elucidate the different proposed mechanisms.

Acknowledgment. The Mexican Consejo Nacional de Ciencia y Tecnología (V.L.), the Fonds der Chemischen Industrie (B.H.), the Alexander von Humboldt Foundation (I.C.), the Deutsche Forschungsgemeinschaft (project GI349 and the Graduate School GK 788 "Hydrogen Bonding and Hydrogen Transfer"), the Deutscher Akademischer Austausch Dienst (Acción Integrada Hispano-Alemana No 12786), and the Spanish Ministerio de Educación y Ciencia (projects CTQ2005-04563 and HA2006-0096) are gratefully acknowledged. The calculations have been performed in the HP workstations of the Theoretical Chemistry Group at the Freie Universität Berlin.

References and Notes

(1) Ciamician, G.; Silber, P. *Ber. Dtsch. Chem. Ges.* **1901**, *34*, 2040.
(2) Roth, H. D. *Pure Appl. Chem.* **2001**, *73*, 395.
(3) George, M. V.; Scaiano, J. C. *J. Phys. Chem.* **1980**, *84*, 492.
(4) Yip, R. W.; Sharma, D. K. *Res. Chem. Intermed.* **1989**, *11*, 109.
(5) Laimgruber, S.; Schreier, W. J.; Schrader, T.; Koller, F.; Zinth, W.; Gilch, P. *Angew. Chem. Int. Ed.* **2005**, *44*, 7901.
(6) Kröhl, O.; Malsch, K.; Swiderek, P. *Phys. Chem. Chem. Phys.* **2000**, *2*, 947.
(7) Molina, V.; Merchán, M. *J. Phys. Chem. A* **2001**, *105*, 3745.
(8) Pelliccioli, A. P.; Wirz, J. *Photochem. Photobiol. Sci.* **2002**, *1*, 441.
(9) Coppens, P.; Schmidt, G. M. J. *Acta Crystallogr.* **1964**, *17*, 222.
(10) Roos, B. O. In *Ab Initio Methods in Quantum Chemistry II*, Lawley, K. P., Ed.; Wiley: Chichester, 1987.
(11) Gross, E. K. U.; Kohn, W. *Adv. Quantum Chem.* **1990**, *21*, 255.
(12) Christiansen, O.; Koch, H.; Jorgensen, P. *Chem. Phys. Lett.* **1995**, *243*, 409.
(13) Hättig, C.; Weigend, F. *J. Chem. Phys.* **2000**, *113*, 5154.
(14) Widmark, P.-O.; Malmqvist, P.-A.; Roos, B. O. *Theor. Chim. Acta* **1990**, *77*, 291.
(15) Finley, J.; Malmqvist, P.-A.; Roos, B. O.; Serrano-Andrés, L. *Chem. Phys. Lett.* **1998**, *288*, 299.
(16) Roos, B. O.; Anderson, K. *Chem. Phys. Lett.* **1995**, *245*, 215.
(17) Karlström, G.; Lindh, R.; Malmqvist, P.-A.; Roos, B. O.; Ryde, U.; Veryazov, V.; Widmark, P.-O.; Cossi, M.; Schimmelpfennig, B.; Neogrady, P.; Seijo, L. *Comput. Mater. Sci.* **2003**, *28*, 222.
(18) Frisch, M. J.; Trucks, G. W.; Schlegel, H. B.; Scuseria, G. E.; Robb, M. A.; Cheeseman, J. R.; Montgomery, J. J. A.; Vreven, T.; Kudin, K. N.; Burant, J. C.; Millam, J. M.; Iyengar, S. S.; Tomasi, J.; Barone, V.; Mennucci, B.; Cossi, M.; Scalmani, G.; Rega, N.; Petersson, G. A.; Nakatsuji, H.; Hada, M.; Ehara, M.; Toyota, K.; Fukuda, R.; Hasegawa, J.; Ishida, M.; Nakajima, T.; Honda, Y.; Kitao, O.; Nakai, H.; Klene, M.; Li, X.; Knox, J. E.; Hratchian, H. P.; Cross, J. B.; Bakken, V.; Adamo, C.; Jaramillo, J.; Gomperts, R.; Stratmann, R. E.; Yazyev, O.; Austin, A. J.; Cammi, R.; Pomelli, C.; Ochterski, J. W.; Ayala, P. Y.; Morokuma, K.; Voth, G. A.; Salvador, P.; Dannenberg, J. J.; Zakrzewski, V. G.; Dapprich, S.; Daniels, A. D.; Strain, M. C.; Farkas, O.; Malick, D. K.; Rabuck, A. D.; Raghavachari, K.; Foresman, J. B.; Ortiz, J. V.; Cui, Q.; Baboul, A. G.; Clifford, S.; Cioslowski, J.; Stefanov, B. B.; Liu, G.; Liashenko, A.; Piskorz, P.; Komaromi, I.; Martin, R. L.; Fox, D. J.; Keith, T.; Al-Laham, M. A.; Peng, C. Y.; Nanayakkara, A.; Challacombe, M.; Gill, P. M. W.; Johnson, B.; Chen, W.; Wong, M. W.; Gonzalez, C.; Pople, J. A. *Gaussian 03*, revision C.02; Gaussian, Inc.: Wallingford, CT, 2004.
(19) Ahlrichs, R.; Bär, M.; Häser, M.; Horn, H.; Kölmel, C. *Chem. Phys. Lett.* **1989**, *162*, 165.
(20) Demtröder, W. *Laser Spectroscopy: Basic Concepts and Instrumentation*; Springer Verlag: Berlin, 2002.
(21) Antonov, L.; Nedeltcheva, D. *Chem. Soc. Rev.* **2000**, *29*, 217.
(22) Berlman, I. B. *Handbook of Fluorescence Spectra of Aromatic Molecules*, 2nd edition; Academic Press: New York, 1971.
(23) Galloway, D. B.; Barth, J. A.; Huey, L. G.; Crim, F. F. *J. Chem. Phys.* **1993**, *98*, 2107.

JP711949J